AGU PUBLICATIONS

Geophysical Research Letters

RESEARCH LETTER
10.1002/2017GL073836

Key Points:
- We introduce a routine for separating relict and recrystallized grains based on characterizing intragranular lattice distortion
- Grain size data from EBSD and light optical microscopy are compared to explore the effect of resolution on grain size measurements
- We define two EBSD-based recrystallized grain size paleopiezometers for quartz

Supporting Information:
- Supporting Information S1
- Data Set S1
- Data Set S2
- Data Set S3

Correspondence to:
D. J. Prior,
david.prior@otago.ac.nz

Citation:
Cross, A. J., D. J. Prior, M. Stipp, and S. Kidder (2017), The recrystallized grain size piezometer for quartz: An EBSD-based calibration, *Geophys. Res. Lett.*, *44*, doi:10.1002/2017GL073836.

Received 15 APR 2017
Accepted 14 JUN 2017
Accepted article online 21 JUN 2017

The recrystallized grain size piezometer for quartz: An EBSD-based calibration

A. J. Cross[1], D. J. Prior[2], M. Stipp[3], and S. Kidder[4]

[1]Department of Earth and Planetary Sciences, Washington University in St. Louis, St. Louis, Missouri, USA, [2]Department of Geology, University of Otago, Dunedin, New Zealand, [3]Institute of Geology, University of Innsbruck, Innsbruck, Austria, [4]Department of Earth and Atmospheric Science, City College of New York, New York, New York, USA

Abstract We have reanalyzed samples previously used for a quartz recrystallized grain size paleopiezometer, using electron backscatter diffraction (EBSD). Recrystallized and relict grains are separated using their grain orientation spread, which acts as a measure of intragranular lattice distortion and a proxy for dislocation density. For EBSD maps made with a 1 μm step size, the piezometer relationship is $D = 10^{3.91 \pm 0.41} \cdot \sigma^{-1.41 \pm 0.21}$ (for root-mean-square mean diameter values). We also present a "sliding resolution" piezometer relationship, $D = 10^{4.22 \pm 0.51} \cdot \sigma^{-1.59 \pm 0.26}$, that combines 1 μm step size data at coarser grain sizes with 200 nm step size data at finer grain sizes. The sliding resolution piezometer more accurately estimates stress in fine-grained (<10 μm) samples. The two calibrations give results within 10% of each other for recrystallized grain sizes between 10 μm and 100 μm. Both piezometers match the original light optical microscopy quartz piezometer within error.

Plain Language Summary Constraining stress magnitudes imposed during the high-temperature creep of rocks in the lithosphere is crucial to our understanding of tectonics. Stress magnitudes can be constrained by their inverse relationship with recrystallized grain size: a method known as paleopiezometry. Quantitative microstructural analysis of deformed rocks is now routinely carried out using electron backscatter diffraction (EBSD): a scanning electron microscope technique. We outline a procedure for quantifying mean recrystallized grain size from EBSD data and provide the first EBSD-based paleopiezometer calibration, in this case for quartz. Our empirical piezometer calibration can be used to robustly quantify stress magnitudes driving quartz deformation at the time of recrystallization.

1. Introduction

Recrystallized grain size paleopiezometry [*Luton and Sellars*, 1969; *Twiss*, 1977; *Ranalli*, 1984; *Stipp et al.*, 2010] provides some of the only constraints on the magnitude of differential stress in the nonseismogenic parts of the lithosphere [*Kohlstedt and Weathers*, 1980; *Hacker et al.*, 1992; *Stipp et al.*, 2002; *Behr and Platt*, 2011; *Kidder et al.*, 2012; *Cross et al.*, 2015a]. Mylonites that are used for paleopiezometry studies often have a population of relict grains and a population of finer recrystallized grains. Separating these populations by a grain size threshold causes a truncation of the grain size distributions at their upper or lower ends, for recrystallized and relict grains, respectively, thereby skewing differential stress estimations [*Lopez-Sanchez and Llana-Funez*, 2015]. Furthermore, this approach becomes increasingly difficult as the recrystallized and relict grain size distributions overlap. For statistical robustness, we need a method of isolating relict and recrystallized grain populations that is independent of the grain size measurement and the degree of overlapping of different grain populations.

Electron backscatter diffraction (EBSD) has become a widely available and well-established method for quantifying rock microstructure [*Prior et al.*, 1999, 2009]. EBSD data can be used to quantify the intensity of intragranular lattice distortion [*Wheeler et al.*, 2009; *Wright et al.*, 2011] and may, therefore, provide an independent method for characterizing grains as relict or recrystallized: we would expect relict grains to have greater internal distortion than recrystallized grains. Indeed, this is the basis of routines used to isolate recrystallized grain fractions in deformed and then recrystallized metals [e.g., *Field et al.*, 2005].

EBSD maps are also commonly used to characterize grain size distributions in mylonites [e.g., *Halfpenny et al.*, 2006; *Cross et al.*, 2015b]. However, the application of EBSD measurements to estimate paleostress values is problematic as no available paleopiezometer is based on EBSD grain size measurements: all use other approaches (e.g., optical microscopy and computer integrated polarization (CIP) [*Heilbronner and Pauli*, 1993]).

Table 1. List of Samples Together With Differential Stress [From *Stipp and Tullis*, 2003; *Stipp et al.*, 2006] Together With EBSD Step Size, Area, Indexing Rate, and Statistics Extracted From EBSD Data[a]

Sample	Stress (MPa)	Step Size	Area (mm^2)	Raw Indexing Rate (%)	Total No. of Grains	No. of Relict Grains	No. of Rex. Grains	Stipp and Tullis d (μm)	EBSD RMS d (μm)	EBSD Arithmetic d (μm)	EBSD Geometric d (μm)	EBSD Median d (μm)	EBSD Mode d (μm)	EBSD Error 1σ (μm)
W1126	34 ± 16	1 μm[b]	3.61	97.1	1064	236	828	46 ± 15	61.0	53.5	45.5	49.0	5.16	29.5
		200 nm	0.096	95.0	64	22	42		25.9	18.1	7.28	6.84	0.939	19.0
W1143	58 ± 18	1 μm[b]	1.40	97.9	1615	255	1360	19.9 ± 4.9	27.5	22.2	18.0	18.1	4.48	16.2
		200 nm	0.096	98.3	99	25	74		26.1	21.0	17.0	17.5	2.82	15.7
W1066	60 ± 15	1 μm[b]	2.70	97.3	5973	1201	4772	18 ± 5.5	18.2	15.9	13.6	14.2	3.39	8.82
		200 nm	0.104	85.1	193	71	122		17.9	15.8	13.6	13.9	3.72	8.61
W1025	87 ± 17	1 μm[b]	2.24	97.1	3639	807	2832	13.6 ± 4.0	18.3	16.0	13.7	14.3	8.46	8.85
		200 nm	0.060	98.2	149	52	97		15.5	13.1	11.0	10.0	2.77	8.37
W1024	102 ± 9	1 μm[b]	1.28	96.4	3832	769	3063	11.6 ± 3.2	12.6	11.0	9.55	9.84	3.04	6.10
		200 nm	0.112	96.8	396	115	281		10.8	9.64	8.54	8.77	1.94	4.94
W1029	130 ± 13	1 μm	1.20	96.0	7491	1328	6163	9.0 ± 2.4	9.83	8.70	7.67	7.74	2.88	4.58
		200 nm[b]	0.104	96.2	739	185	554		8.37	7.44	6.58	6.61	1.51	3.83
W1081	139 ± 24	1 μm[b]	0.898	96.6	2339	497	1842	6.9 ± 2.0	7.34	6.57	5.89	5.88	2.82	3.27
		200 nm	0.096	97.5	238	82	156		6.13	5.45	4.81	4.74	1.11	2.82
W1050	149 ± 18	1 μm	0.894	93.7	6104	762	5342	5.0 ± 1.3	6.09	5.32	4.81	4.58	2.52	2.97
		200 nm[b]	0.086	91.9	943	234	709		4.63	4.14	3.71	3.65	0.492	2.07
W1051	189 ± 30	1 μm	0.905	85.0	8641	1114	7527	4.6 ± 1.1	5.03	4.61	4.32	4.13	2.28	2.01
		200 nm[b]	0.096	89.4	1449	299	1150		3.53	3.19	2.89	2.89	0.711	1.51

[a]Measurement errors in differential stress and grain size (1 standard deviation) are indicated.
[b]EBSD data used to define the sliding resolution piezometer.

Here we define two EBSD-based piezometers for quartz by reanalyzing samples used to calibrate the empirical piezometer of *Stipp and Tullis* [2003] and *Stipp et al.* [2006], using internal distortion to separate relict and recrystallized grain populations.

2. Materials and Methods

We reanalyzed, using EBSD, nine of the experimental samples that were originally deformed and analyzed by *Stipp and Tullis* [2003] and *Stipp et al.* [2006] to define a quartz recrystallized grain size piezometer. Samples are listed in Table 1, and experimental details are summarized by *Stipp et al.* [2006]. The original Stipp and Tullis thin sections were polished with colloidal silica [*Lloyd*, 1987] and coated with a thin layer (~5 nm) of carbon. EBSD data were collected on a Zeiss SIGMA VP field emission gun scanning electron microscope using 30 kV accelerating voltage and ~90 nA beam current. EBSD patterns were collected on a NordlysF camera and processed and indexed using Oxford Instruments AZTEC software. Each sample was mapped at reconnaissance scale (10–30 μm step size) to select an area of about 2 by 0.7 mm: roughly equivalent to the area occupied by 300 grains in the undeformed Black Hills Quartzite starting material (69 ± 24 μm mean grain size) [*Stipp and Kunze*, 2008]. This area was mapped with a 1 μm step size, before a subarea of about 0.7 by 0.2 mm was mapped at a 200 nm step size.

The raw data are of a very high quality (Figure 1) with >95% of pixels typically indexed (Table 1) and a negligible misindexing rate. Data collection rates were about 25 patterns per second. After EBSD mapping, rectangular areas of contamination were visible in the optical microscope and correspond to the areas scanned by the beam during EBSD mapping. We measured the dimensions of these rectangles and compared them with the dimensions of the EBSD maps to estimate the magnitude of distortion (related to the electron optics) in the SEM images and EBSD data. There is a small distortion; however, the impact on any grain size measurements is less than 1%, so no corrections were made.

Grains are constructed from raw EBSD pixel data using a Voronoi decomposition algorithm [*Bachmann et al.*, 2011] implemented within the open-source MTEX toolbox for MATLAB (http://mtex-toolbox.github.io/). We allow full interpolation of the data (to fill in all nonindexed space) and define high-angle grain boundaries by a critical misorientation of 10° [*White and White*, 1981; *Shigematsu et al.*, 2006]. Next, we remove grains comprised of 1 pixel (wild spikes) and then reconstruct grains using the same parameters as before. Dauphiné twin boundaries are removed by merging grains separated by a 60° ± 5° rotation around the

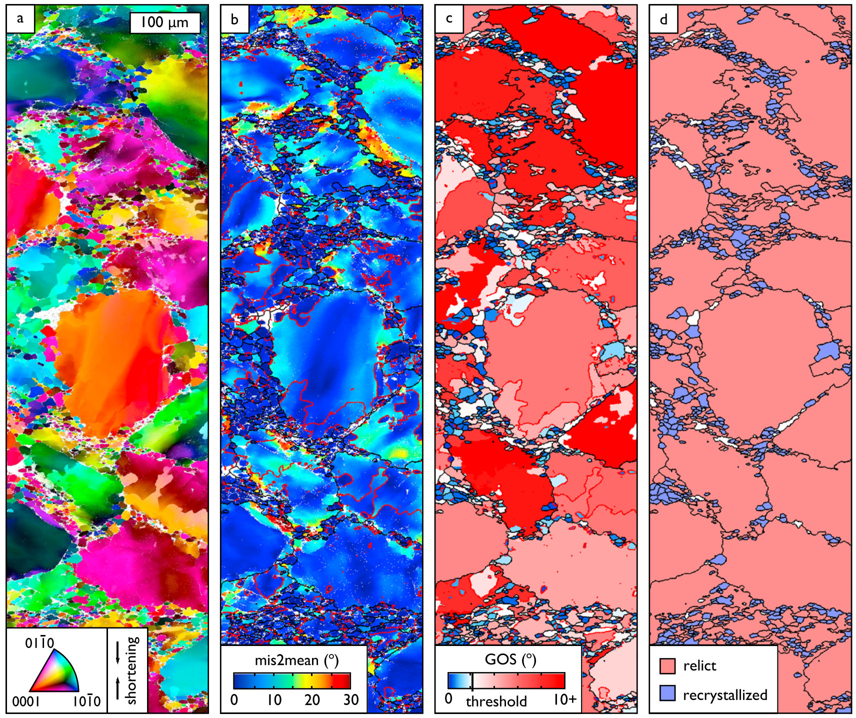

Figure 1. Example EBSD map data, from sample W1051 (189 MPa), collected with a 200 nm step size. (a) Inverse pole figure (IPF) map showing crystal orientations with respect to the shortening axis (vertical). (b) Map of the misorientation between each pixel and the mean orientation of their parent grain (mis2mean). Black lines are grain boundaries; red lines are Dauphiné twin boundaries. (c) Grain orientation spread (GOS) for each grain, colored relative to the GOS threshold (white) between recrystallized (blue) and relict (red) grains. (d) GOS-separated recrystallized and relict grains; twin boundaries have been removed. White areas are poorly indexed and excluded from the analysis.

$<$0001$>$ axis. Although Dauphiné twins may play a role in recrystallization [*Lloyd*, 2004; *Stipp and Kunze*, 2008; *Menegon et al.*, 2011], they are not visible using light optics and have been excluded here to provide best comparison with the original piezometer.

By allowing full interpolation of the data in the Voronoi grain definition algorithm, a small number of poorly constrained grains are produced in regions of sparse pixel coverage. We remove these grains based on the fraction of their area covered by indexed pixels, following the methodology introduced by *Cross et al.* [2015a]. Grains containing fewer than 4 indexed pixels were also removed, as these may result from misindexing. An example of a resultant grain population is shown in Figure 1d.

Recrystallized (i.e., low strain) grains are separated from relict (i.e., high strain) grains by quantifying the degree of intracrystalline lattice distortion in each grain. Intracrystalline lattice distortion is proportional to dislocation density and can be visualized using the MTEX "mis2mean" property (Figure 1b), which gives the misorientation angle between every pixel in a grain and the mean orientation of that grain. We calculate the grain orientation spread (GOS) of each grain (Figure 1c), which is equivalent to the average mis2mean value of each grain [*Wright et al.*, 2011] (Figure S1) and is insensitive to the EBSD indexing rate and step size (see Text and Figure S1 in the supporting information). Next, we use a trade-off curve to calculate a threshold GOS value, which separates recrystallized and relict grains (Figure 2a). Plotting the GOS threshold versus differential stress for all samples (Figure 2b) reveals a positive correlation, reflecting an overall increase in lattice distortion with stress, corresponding to an increase in dislocation density.

Figure 3 shows the separated relict (red; GOS $>$ threshold) and recrystallized (blue; GOS $<$ threshold) grain populations for a low and high stress sample. Figure 1d illustrates these populations on an EBSD map for the high stress sample. An average recrystallized grain size is quantified by removing all border grains (grains that are truncated at the map edge) and calculating the root mean square (RMS) of the remaining recrystallized grains. No stereological correction is made here. The RMS grain size is used for consistency with the original *Stipp and Tullis* [2003] dislocation creep regime 2–3 piezometer of quartz.

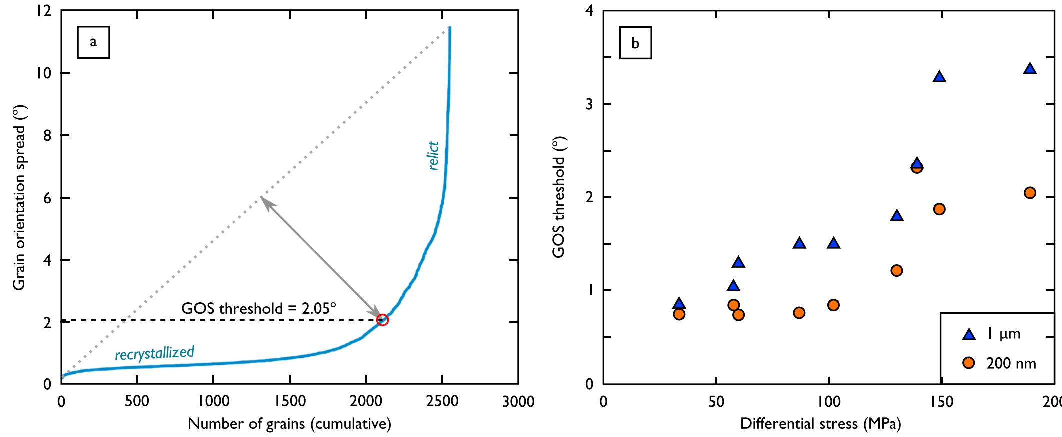

Figure 2. (a) A cumulative plot of the number of grains versus the grain orientation spread (GOS). The knee in the curve (the point furthest from a line connecting the ends of the trade-off curve) gives the threshold between recrystallized and relict grains. (b) Plotting differential stress versus the GOS threshold for the nine experiments reveals a positive correlation reflecting an overall increase in intragranular distortion with stress.

3. Results: Separation of Relict and Recrystallized Grain Populations

Maps of relict and recrystallized grains (Figure 1d) and grain size distributions (Figure 3) for all samples, both from 1 µm and 200 nm step size data, are shown in Figure S2. RMS and other statistical measures of average grain size are listed in Table 1. In all cases, visual inspection of the maps and grain size histograms suggest that the GOS-based separation of recrystallized grains is reasonable. Grains defined as recrystallized grains are all small. Relict grains are mostly large but include a significant population of small grains. Some of these small relict grains may represent recrystallized grains that formed early in the deformation history and

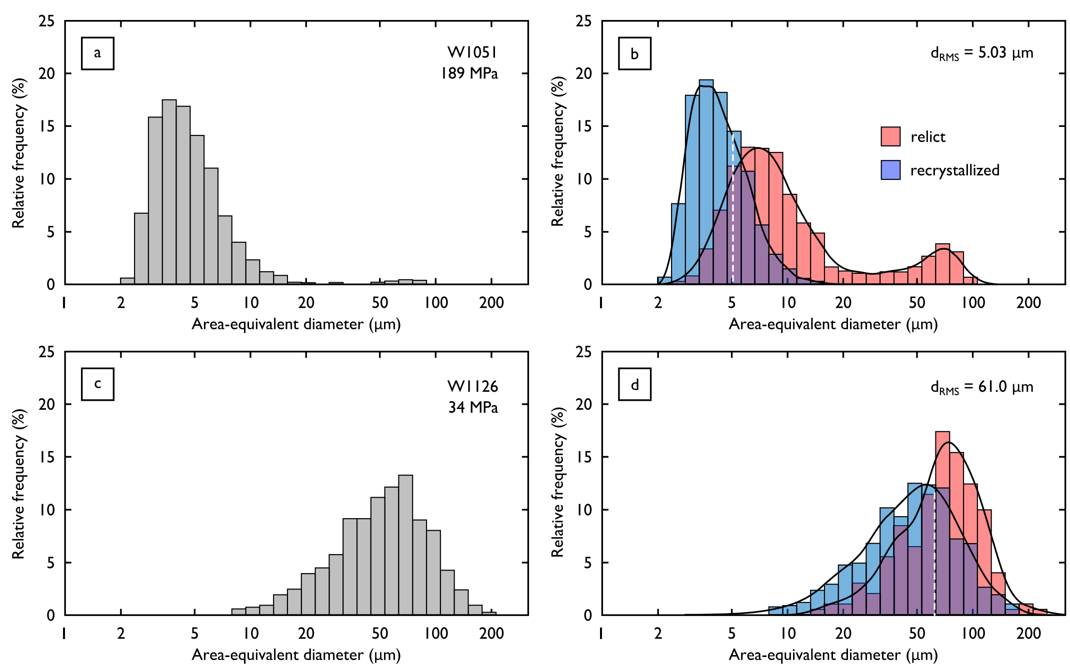

Figure 3. Log_{10} grain size distributions for (a and b) high stress (W1051; 189 MPa) and (c and d) low stress (W1126; 34 MPa) example data sets. Figures 3a and 3c are the grain size distributions for the entire grain population, which are separated into relict and recrystallized grain size distributions in Figures 3b and 3d. Relative frequencies (Figures 3b and 3d) are calculated with respect to the number of grains in each subpopulation, to “amplify” the relict grain histograms (red) which have a low relative abundance. Histograms are fitted with kernel density estimator functions for comparison with the RMS recrystallized grain size (white dashed line).

subsequently accumulated strain. Additionally, some of the small relict grains may belong to larger relict grains in three dimensions. A rough estimate of the proportion of apparently small (i.e., due to a cutting effect) relict grains can be made by drawing intercept lines on an EBSD map. For the map in Figure 1, approximately 20–25% of relict grains have intercept lengths less than one fifth of the maximum diameter measured for that grain. In contrast, 80% of the relict grain population overlaps the recrystallized grain population (Figure 3a). These observations are consistent with the proportion of small relict grains measured in two dimensions being a true reflection of the proportion in three dimensions. Comparisons of 2-D and 3-D mylonite microstructure data sets [*Berger et al.*, 2011] give similar results.

The GOS method is effective at deconvolving two overlapping grain size distributions, assuming that the two grain populations have quantifiably different magnitudes of internal distortion (dislocation density), as would be expected for experimentally or naturally deformed samples containing an original population of quartz grains that are not fully recrystallized [*Hirth and Tullis*, 1992] or for statically recrystallized deformed metals [*Field et al.*, 2005]. In theory, this method should be particularly useful at low stresses where bulk grain size distributions appear unimodal (Figure 3c), such that separating relict and recrystallized grains would not be robust with a conventional grain size cutoff method and would be difficult by other purely statistical means. In practice, however, the degree of error increases as stress decreases because the amount of intragranular misorientation approaches the angular resolution limit (nominally ~0.5°) of conventional EBSD [*Humphreys*, 2004]. This effect may compromise grain separation in the lowest-stress sample presented here (W1126), where recrystallized grain sizes are very similar to those of the starting material used in these experiments. However, sample W1126 exhibits optically visible subgrains and grain boundary bulges that are not present in the starting material [see *Stipp and Kunze*, 2008], as well as low-GOS (recrystallized) grains that are similar in size to these features. These microstructures imply that the grain separation in W1126 is robust, and not an artifact of local variations in EBSD indexing accuracy. Nevertheless, we suggest that high angular resolution operating procedures [*Prior et al.*, 1999; *Wilkinson et al.*, 2010; *Wallis et al.*, 2016] should give improved performance for lower stress samples.

The GOS method has a slight grain size bias (Figure S1), which yields higher GOS values for larger grains. This bias is minor and has little impact on the ability to separate recrystallized and relict populations: critically, the GOS-based separation of grains will be robust at the overlap of the grain size distributions where relict and recrystallized grains have similar sizes. In the future it may be worth incorporating fully scaled measures of lattice distortion, such as the weighted mean burgers vector (WMBV) [*Wheeler et al.*, 2009]. At present, software tools are not available to apply the WMBV approach automatically to large data sets.

Additional bias in the GOS method may arise from differences in dislocation density related to crystal orientation (i.e., hard versus soft orientations) [*Kilian and Heilbronner*, 2017]. However, the samples analyzed here have generally weak crystallographic preferred orientations (CPOs) and show no correlation between grain orientation and GOS value (Figure S3).

4. Results: EBSD-Based Quartz Recrystallized Grain Size Piezometers

RMS mean recrystallized grain sizes for the 1 μm and 200 nm step size data are plotted against differential stress in Figure 4a. The 200 nm step size data yield smaller recrystallized grain sizes than those measured by *Stipp and Tullis* [2003], while lower resolution (1 μm) maps yield larger recrystallized grain sizes, implying an effective CIP resolution somewhere in between. Indeed, when working with ultrathin sections as done by *Stipp and Tullis* [2003], the CIP resolution is largely controlled by the optical spectrum of around 400 to 700 nm. The largest discrepancies between EBSD and CIP grain sizes occur in lower stress samples, where recrystallized grains are coarser. This is likely because the distinction of relict and recrystallized grains (see Figures 3c and 3d) is much harder in these samples, for both optical and electron microscopy methods. However, both the 1 μm and 200 nm step size data overlap with the original *Stipp and Tullis* [2003] CIP-based piezometer within error of the recrystallized grain size and differential stress estimation (Figure 4a).

An "EBSD 1 μm RMS piezometer" is calculated from the best fit equation to the 1 μm data ($D = 10^{3.91 \pm 0.41} \cdot \sigma^{-1.41 \pm 0.21}$). The 200 nm data do not provide a robust piezometer when used in isolation, because most maps contain fewer than 300 grains. Expanding the size of 200 nm maps to get robust

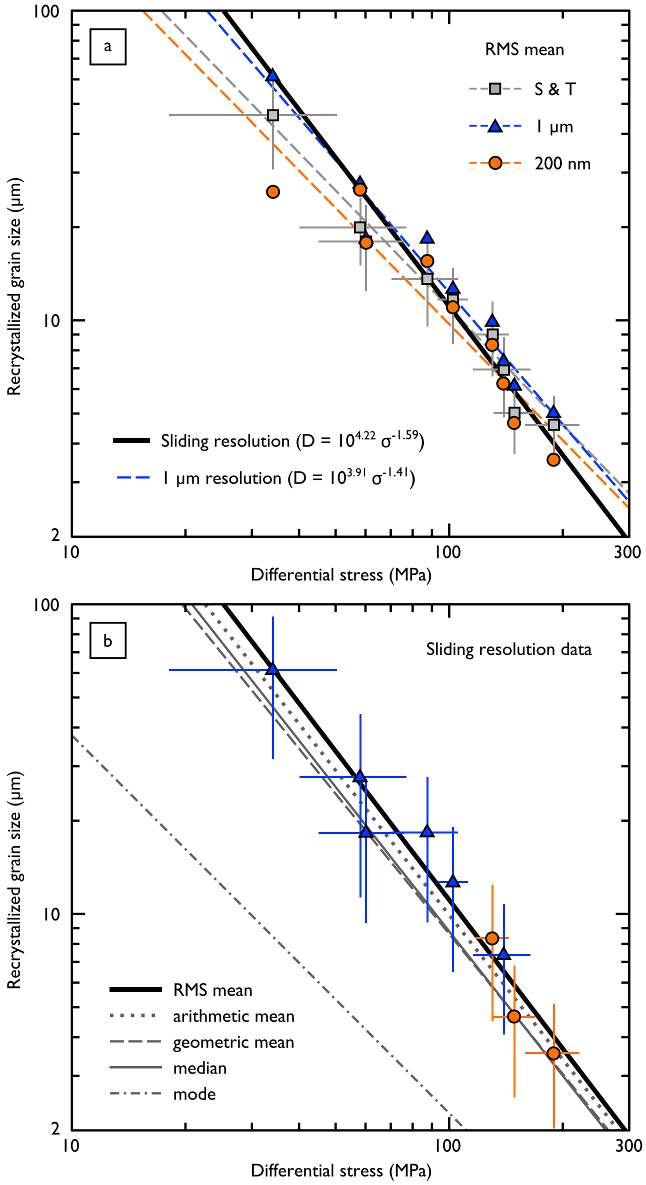

Figure 4. Log-log plots of recrystallized grain size versus differential stress. (a) The published RMS recrystallized grain sizes measured by CIP [*Stipp and Tullis*, 2003] (dashed grey line), and the RMS mean grain sizes for EBSD defined recrystallized grains extracted from 1 μm (dashed blue) and 200 nm (dashed orange) step size EBSD data. The sliding resolution RMS piezometer, which incorporates data from the 200 nm maps at the highest stresses, is shown in black. (b) The sliding resolution piezometer calculated from RMS, arithmetic and geometric means, and the median and mode data (equations for all are given in the supporting information Table S1). Error bars are shown for the Stipp and Tullis CIP data (Figure 4a) and the sliding resolution EBSD data (Figure 4b).

statistics is impractical, as each of these maps would require several days to complete. However, at mean recrystallized grain sizes of <10 μm, the 1 μm maps do not capture all recrystallized grains and overestimate the mean grain size. In order to account for these resolution effects, we have defined an "EBSD sliding resolution RMS piezometer" ($D = 10^{4.22 \pm 0.51} \cdot \sigma^{-1.59 \pm 0.26}$) that uses the 200 nm data where the recrystallized grain population contains >300 grains (W1029, W1050, and W1051), and the 1 μm data for all other samples (Figure 4b). The EBSD 1 μm RMS piezometer and the EBSD sliding resolution RMS piezometer give stresses that match to within 10% for recrystallized grain sizes between 10 μm and 100 μm.

The EBSD sliding resolution RMS piezometer implies a slightly greater stress sensitivity of grain size than that reflected in either the EBSD 1 μm RMS piezometer or the CIP-based piezometer [*Stipp and Tullis*, 2003]. To investigate this, we have performed analyses to test the effect of EBSD resolution (i.e., step size) on the stress sensitivity of the piezometer. In Figure S4, the 1 μm step size data have been artificially degraded to produce data with 2 μm, 5 μm, and 10 μm step sizes. As step size increases, the minimum resolvable grain size increases. Consequently, estimated recrystallized grain sizes become increasingly overestimated in the higher stress data, as the "true" recrystallized grain sizes fall below resolution limit of the degraded data (Figure S5). These results demonstrate that the piezometer with the greatest stress sensitivity (the sliding resolution piezometer, in this case) is that which most reliably captures recrystallized grains, particularly at high stresses.

If the sliding resolution piezometer is used, EBSD maps should be collected at a step size that captures all grains in the population. Inspection of our data suggests that the step size needs to be smaller than one fifth of the diameter of smallest grains in the recrystallized grain size population. Piezometers derived using other statistical measures [*Ranalli*, 1984; *Berger et al.*, 2011] of average grain size are calculated from the same data used to calculate the sliding resolution piezometer and are shown on Figure 4b for comparison.

We recommend the following treatment of EBSD data for obtaining paleostress estimates in quartz mylonites:

1. Collect EBSD maps at a step size that allows measurement of all recrystallized grains. Step size should be smaller than one fifth the diameter of the smallest recrystallized grains.
2. Use the grain orientation spread (GOS) to separate relict and recrystallized grains (ideally following the procedure outlined above) and calculate a mean recrystallized grain size. The MTEX script used here is included in the supporting information ("RexRelict.m").
3. If mean recrystallized grain sizes are greater than 10 μm, then either the EBSD 1 μm RMS piezometer or the EBSD sliding resolution RMS piezometer can be used. If recrystallized grain sizes are less than 10 μm, the EBSD sliding resolution RMS piezometer is recommended.

The methods outlined here are applicable to samples where there is a clear relict grain and recrystallized grain population. In completely recrystallized samples, differential stress can be found by taking the mean grain size without the need for grain separation. In naturally deformed samples the method is applicable to samples with bulging and subgrain rotation recrystallization microstructures following *Stipp et al.* [2002, 2010]. Significant caution is needed in applying these methods to samples where dislocation densities are low, for example, within the high-temperature, grain boundary migration regime for quartz [e.g., *Little et al.*, 2015]. In all cases, caution should be exercised to ensure that the mean grain size accurately represents the recrystallized grain population. Specifically, the mean recrystallized grain size should lie close to the peak of a unimodal recrystallized grain size distribution [*Lopez-Sanchez and Llana-Funez*, 2015]. In scenarios where the smallest grains are not measured, or where a subpopulation of larger grains is included in the analysis, mean values will overestimate grain size and, therefore, underestimate stress.

EBSD calibrations would be very useful for other commonly applied recrystallized grain size piezometers [*Schmid et al.*, 1980; *Van der Wal et al.*, 1993; *Rutter*, 1995; *Post and Tullis*, 1999]. The procedures outlined here provide a framework for establishing EBSD-based piezometers for other crystalline materials. The EBSD data also provide a good foundation to assess the role of specific material processes and driving forces in controlling the (recrystallized) grain size-stress relationship [*De Bresser et al.*, 2001; *Austin and Evans*, 2007].

5. Conclusions

1. The grain orientation spread (GOS) provides a measure of intragranular lattice distortion that is largely grain size independent. The GOS can be used to distinguish relict grain and recrystallized grain populations in quartz samples (and likely in other mineral phases also), in cases where the two populations have quantifiably different magnitudes of intragranular lattice distortion.
2. We have provided methods and calibrations for two EBSD-based quartz recrystallized grain size piezometers. A calibration (EBSD 1 μm RMS piezometer) is provided for EBSD data collected with a 1 μm step size. Use of the EBSD sliding resolution RMS piezometer requires that data are collected at a step size that captures the entire grain population: we recommend using a step size smaller than one fifth of the diameter of the smallest recrystallized grains.
3. The EBSD-based quartz recrystallized grain size piezometers match the published piezometer of *Stipp and Tullis* [2003] within experimental error. The biggest differences between calibrations are at low stresses and large recrystallized grain sizes where the magnitude of intragranular lattice distortion is below the angular resolution of conventional EBSD.

Acknowledgments
A pilot study of these samples, which led directly to this work, was carried out by Vicki O'Connor for a fourth-year project at the University of Liverpool. Marsden Fund UOO1116, granted to Prior by the Royal Society of New Zealand, supported the detailed work presented here. Brent Pooley repolished the samples. Kat Lilly, Marco Brenna, and Richard Easingwood provided SEM support. We are indebted to Jan Tullis, whose work on the original quartz piezometer calibration made this study possible. This manuscript benefited from constructive reviews by Luca Menegon and Sergio Llana-Fúnez. The EBSD data presented here can be obtained upon request from the authors.

References

Austin, N. J., and B. Evans (2007), Paleowattmeters: A scaling relation for dynamically recrystallized grain size, *Geology*, *35*(4), 343–346, doi:10.1130/G23244A.1.

Bachmann, F., R. Hielscher, and H. Schaeben (2011), Grain detection from 2d and 3d EBSD data—Specification of the MTEX algorithm, *Ultramicroscopy*, *111*(12), 1720–1733, doi:10.1016/j.ultramic.2011.08.002.

Behr, W. M., and J. P. Platt (2011), A naturally constrained stress profile through the middle crust in an extensional terrane, *Earth Planet. Sci. Lett.*, *303*(3–4), 181–192.

Berger, A., M. Herwegh, J.-O. Schwarz, and B. Putlitz (2011), Quantitative analysis of crystal/grain sizes and their distributions in 2D and 3D, *J. Struct. Geol.*, *33*(12), 1751–1763, doi:10.1016/j.jsg.2011.07.002.

De Bresser, J., J. Ter Heege, and C. Spiers (2001), Grain size reduction by dynamic recrystallization: Can it result in major rheological weakening?, *Int. J. Earth Sci.*, *90*(1), 28–45, doi:10.1007/s005310000149.

Cross, A. J., S. Kidder, and D. J. Prior (2015a), Using microstructures and TitaniQ thermobarometry of quartz sheared around garnet porphyroclasts to evaluate microstructural evolution and constrain an Alpine Fault Zone geotherm, *J. Struct. Geol.*, *75*, 17–31, doi:10.1016/j.jsg.2015.02.012.

Cross, A. J., S. Ellis, and D. J. Prior (2015b), A phenomenological numerical approach for investigating grain size evolution in ductiley deforming rocks, *J. Struct. Geol.*, *76*, 22–34, doi:10.1016/j.jsg.2015.04.001.

Field, D. P., M. M. Nowell, P. Trivedi, S. I. Wright, and T. M. Lillo (2005), Local orientation gradient and recrystallization of deformed copper, *Solid State Phenom.*, *105*, 157–162, doi:10.4028/www.scientific.net/SSP.105.157.

Hacker, B. R., A. Yin, J. M. Christie, and G. A. Davis (1992), Stress magnitude, strain rate, and rheology of extended Middle Continental Crust inferred from quartz grain sizes in the Whipple Mountains, California, *Tectonics*, *11*(1), 36–46, doi:10.1029/91TC01291.

Halfpenny, A., D. J. Prior, and J. Wheeler (2006), Analysis of dynamic recrystallization and nucleation in a quartzite mylonite, *Tectonophysics*, *427*(1–4), 3–14, doi:10.1016/j.tecto.2006.05.016.

Heilbronner, R. P., and C. Pauli (1993), Integrated spatial and orientation analysis of quartz c-axes by computer-aided microscopy, *J. Struct. Geol.*, *15*(3–5), 369–382, doi:10.1016/0191-8141(93)90133-U.

Hirth, G., and J. Tullis (1992), Dislocation creep regimes in quartz aggregates, *J. Struct. Geol.*, *14*(2), 145–159, doi:10.1016/0191-8141(92)90053-Y.

Humphreys, F. (2004), Characterisation of fine-scale microstructures by electron backscatter diffraction (EBSD), *Scr. Mater.*, *51*(8), 771–776, doi:10.1016/j.scriptamat.2004.05.016.

Kidder, S., J.-P. Avouac, and Y.-C. Chan (2012), Constraints from rocks in the Taiwan orogen on crustal stress levels and rheology, *J. Geophys. Res.*, *117*, B09408, doi:10.1029/2012JB009303.

Kilian, R., and R. Heilbronner (2017), Texture analysis of experimentally deformed Black Hills quartzite, *Solid Earth Discuss.*, 1–62, doi:10.5194/se-2017-44.

Kohlstedt, D. L., and M. S. Weathers (1980), Deformation-induced microstructures, paleopiezometers, and differential stresses in deeply eroded fault zones, *J. Geophys. Res.*, *85*(B11), 6269–6285, doi:10.1029/JB085iB11p06269.

Little, T. A., D. J. Prior, V. G. Toy, and Z. R. Lindroos (2015), The link between strength of lattice preferred orientation, second phase content and grain boundary migration: A case study from the Alpine Fault zone, New Zealand, *J. Struct. Geol.*, *81*, 59–77, doi:10.1016/j.jsg.2015.09.004.

Lloyd, G. E. (1987), Atomic-number and crystallographic contrast images with the SEM: A review of backscattered electron techniques, *Mineral. Mag.*, *51*(359), 3–19.

Lloyd, G. E. (2004), Microstructural evolution in a mylonitic quartz simple shear zone: The significant roles of dauphine twinning and misorientation, *Geol. Soc. London, Spec. Publ.*, *224*(1), 39–61, doi:10.1144/GSL.SP.2004.224.01.04.

Lopez-Sanchez, M. A., and S. Llana-Funez (2015), An evaluation of different measures of dynamically recrystallized grain size for paleopiezometry or paleowattometry studies, *Solid Earth*, *6*, 475–495.

Luton, M., and C. Sellars (1969), Dynamic recrystallization in nickel and nickel-iron alloys during high temperature deformation, *Acta Metall.*, *17*(8), 1033–1043, doi:10.1016/0001-6160(69)90049-2.

Menegon, L., S. Piazolo, and G. Pennacchioni (2011), The effect of Dauphiné twinning on plastic strain in quartz, *Contrib. Mineral. Petrol.*, *161*(4), 635–652, doi:10.1007/s00410-010-0554-7.

Post, A., and J. Tullis (1999), A recrystallized grain size piezometer for experimentally deformed feldspar aggregates, *Tectonophysics*, *303*(1–4), 159–173, doi:10.1016/S0040-1951(98)00260-1.

Prior, D. J., et al. (1999), The application of electron backscatter diffraction and orientation contrast imaging in the SEM to textural problems in rocks, *Am. Mineral.*, *84*(11–12), 1741–1759, doi:10.2138/am-1999-11-1204.

Prior, D. J., E. Mariani, and J. Wheeler (2009), EBSD in the Earth Sciences: Applications, common practice, and challenges, in *Electron Backscatter Diffraction in Materials Science*, pp. 345–360, Springer, Boston, Mass.

Ranalli, G. (1984), Grain size distribution and flow stress in tectonites, *J. Struct. Geol.*, *6*(4), 443–447, doi:10.1016/0191-8141(84)90046-4.

Rutter, E. H. (1995), Experimental study of the influence of stress, temperature, and strain on the dynamic recrystallization of Carrara marble, *J. Geophys. Res.*, *100*(B12), 24,651–24,663, doi:10.1029/95JB02500.

Schmid, S. M., M. S. Paterson, and J. N. Boland (1980), High temperature flow and dynamic recrystallization in carrara marble, *Tectonophysics*, *65*(3–4), 245–280, doi:10.1016/0040-1951(80)90077-3.

Shigematsu, N., D. J. Prior, and J. Wheeler (2006), First combined electron backscatter diffraction and transmission electron microscopy study of grain boundary structure of deformed quartzite, *J. Microsc.*, *224*(3), 306–321, doi:10.1111/j.1365-2818.2006.01697.x.

Stipp, M., and K. Kunze (2008), Dynamic recrystallization near the brittle-plastic transition in naturally and experimentally deformed quartz aggregates, *Tectonophysics*, *448*(1–4), 77–97, doi:10.1016/j.tecto.2007.11.041.

Stipp, M., and J. Tullis (2003), The recrystallized grain size piezometer for quartz, *Geophys. Res. Lett.*, *30*(21), 2088, doi:10.1029/2003GL018444.

Stipp, M., H. Stünitz, R. Heilbronner, and S. M. Schmid (2002), Dynamic recrystallization of quartz: Correlation between natural and experimental conditions, *Geol. Soc. London, Spec. Publ.*, *200*(1), 171–190, doi:10.1144/GSL.SP.2001.200.01.11.

Stipp, M., J. Tullis, and H. Behrens (2006), Effect of water on the dislocation creep microstructure and flow stress of quartz and implications for the recrystallized grain size piezometer, *J. Geophys. Res.*, *111*, B04201, doi:10.1029/2005JB003852.

Stipp, M., J. Tullis, M. Scherwath, and J. H. Behrmann (2010), A new perspective on paleopiezometry: Dynamically recrystallized grain size distributions indicate mechanism changes, *Geology*, *38*(8), 759–762, doi:10.1130/G31162.1.

Twiss, R. J. (1977), Theory and applicability of a recrystallized grain size paleopiezometer, in *Stress in the Earth*, pp. 227–244, Birkhäuser Basel, Basel.

Van der Wal, D., P. Chopra, M. Drury, and J. F. Gerald (1993), Relationships between dynamically recrystallized grain size and deformation conditions in experimentally deformed olivine rocks, *Geophys. Res. Lett.*, *20*(14), 1479–1482, doi:10.1029/93GL01382.

Wallis, D., L. N. Hansen, T. Ben Britton, and A. J. Wilkinson (2016), Geometrically necessary dislocation densities in olivine obtained using high-angular resolution electron backscatter diffraction, *Ultramicroscopy*, *168*, 34–45, doi:10.1016/j.ultramic.2016.06.002.

Wheeler, J., E. Mariani, S. Piazolo, D. J. Prior, P. Trimby, and M. R. Drury (2009), The weighted burgers vector: A new quantity for constraining dislocation densities and types using electron backscatter diffraction on 2D sections through crystalline materials, *J. Microsc.*, *233*(3), 482–494, doi:10.1111/j.1365-2818.2009.03136.x.

White, J. C., and S. H. White (1981), On the structure of grain boundaries in tectonites, *Tectonophysics*, *78*(1–4), 613–628, doi:10.1016/0040-1951(81)90032-9.

Wilkinson, A. J., E. E. Clarke, T. B. Britton, P. Littlewood, and P. S. Karamched (2010), High-resolution electron backscatter diffraction: An emerging tool for studying local deformation, *J. Strain Anal. Eng. Des.*, *45*(5), 365–376, doi:10.1243/03093247JSA587.

Wright, S. I., M. M. Nowell, and D. P. Field (2011), A Review of strain analysis using electron backscatter diffraction, *Microsc. Microanal.*, *17*(3), 316–329, doi:10.1017/S1431927611000055.